Turkish Journal of Electrical Engineering & Computer Sciences

http://journals.tubitak.gov.tr/elektrik/

Research Article

Turk J Elec Eng & Comp Sci
(2018) 26: 1587 – 1598

doi:10.3906/elk-1708-68

Performance analysis of radial and axial flux PMSM based on 3D FEM modeling

Oussama BOUAZIZ[1,2,*], **Imen JAAFAR**[1], **Faouzi BEN AMMAR**[1]
[1]University of Carthage MMA Laboratory, National Institute of Applied Science and Technology (INSAT), Tunis, Tunisia
[2]National Engineering School of Tunis (ENSIT), University of Tunis, Tunisia

Received: 06.08.2017 • **Accepted/Published Online:** 09.01.2018 • **Final Version:** 30.05.2018

Abstract: The objective of this paper is presenting a comparative performance analysis between axial flux and radial flux permanent magnet synchronous machines (PMSMs) dedicated to a 550-W wind turbine application. The outer diameter is fixed for both structures and the modeling is carried out in 3D by means of the finite element method (FEM) using the Multiphysics program ANSYS. The performances of the axial flux and radial flux machines for the same output power and at the same rotor speed are evaluated by comparing their efficiency regarding the material consumption of the active parts and eventually predicting their costs. The obtained results promote the axial flux topology as the best solution for small-scale wind turbine applications.

Key words: Axial flux machine, radial flux machine, finite element analysis, 3D design

1. Introduction

Particular interest is now given to small-scale wind generator technology targeting both rural and urban zones. Direct drive permanent magnet (PM) generators have been increasingly used in the last decade for such applications [1]. In order to obtain high power density, neodymium permanent magnets are considered as powerful and reliable exciter systems in electrical generators [2]. These PM generators can be operated in low and variable speed applications. There are two types of PM machines for electrical wind generators [3]: the radial flux permanent magnet synchronous machine (RF-PMSM) presented in Figure 1a and the axial flux permanent magnet synchronous machine (AF-PMSM) presented in Figure 1b.

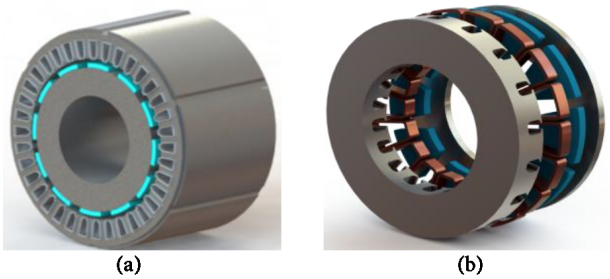

Figure 1. PM generators: a) RF-PMSM, b) AF-PMSM.

PMSMs have some advantages including compact structure, higher torque capability, higher efficiency

*Correspondence: bouaziz.oussama@gmail.com

due to absence of rotor windings and excitation losses, and higher power density than induction machines [4–6]. Because of the discovery of new materials, improvement in manufacturing technology, and innovation, AF-PMSMs are widely used and are recognized as having better power density than RF-PMSMs and being more compact [7,8]. In addition, they have a better ventilation and cooling arrangement. Moreover, AF-PMSMs offer a higher torque-to-weight ratio due to the application of less core material, smaller size, planar and easily adjustable air gap, lower noise, and lower vibration, which make it superior to radial flux machines [9,10].

In [11], the authors developed in detail sizing equations in order to compare the axial and radial flux structures. They concluded that the axial PM structure has a reduced volume compared to the standard radial one. In [12], the authors conducted a comparison between the two topologies and found that the axial flux motor has better torque than the radial flux motor. However, in [13], the comparison between the two machines included the mechanical constraints and the cost of the active parts. The comparison showed that the axial flux cost less than the radial flux but the two topologies had fewer defined parameters in common.

To carry out such studies, researchers are moving towards the application of numerical finite element analysis. Many advanced programs have emerged to offer users the ability to model and analyze electrical machines using two-dimensional (2D) or three-dimensional (3D) designs based on the ?nite element method (FEM) [14–17]. Furthermore, the axial disk type machine has an inherent 3D geometry from the point of view of modeling, so to be rigorous in a study, both radial and axial structures should be modeled and analyzed in 3D.

In this paper, two PMSM architectures are presented. First the design specifications for the stator, rotor, and magnets of both machines with the same output power of 550 W and the adopted winding are presented in order to model the 3D geometries of the machines based on finite element analysis using the ANSYS environment. After that, the materials used for the active parts are assigned and the mesh strategy is applied. Then the magnetic flux density, the magnetic strength, the torque, the different losses, and the evolution of the stator current and EMF for the two machines are discussed. Finally, the cost of the axial and radial machines is estimated based on the material consumption of the different active parts.

2. Design consideration

In the design approach, numerous constraints are necessary to determine the geometry of the components, such as the rated/max speed, the rated/max torque, the phase current, the line-to-line voltage, etc. By neglecting the stator leakage inductance and resistance, the output power of the PMSM is determined by Eq. (1):

$$P_{out} = \eta \frac{m}{T} \int_0^T e(t) i(t) dt = \eta m K_p E_{\max} I_{\max}, \tag{1}$$

where η is the machine efficiency, m is the number of phases, T is the period of one EMF cycle, e(t) is the air gap EMF, and i(t) is the phase current.

E_{max} is the peak of phase air gap, which can be expressed by:

$$E_{\max} = \begin{cases} K_e N_t B_g \frac{f}{p} r_r D_0 L_e & (RF - PMSM) \\ K_e N_t B_g \frac{f}{p} \left(1 - r_a^2\right) D_0^2 & (AF - PMSM) \end{cases}, \tag{2}$$

where N_t is the number of turns per phase, B_g is the flux density in the air gap, f is the operating frequency, p is the machine pole pairs, r_r is the diameter ratio for the radial flux machine, r_a is the diameter ratio for

the axial flux machine with diameter ratio r defined as the inner diameter D_{in} divided by the outer diameter D_{out}, and L_e is the effective stack length of the machine.

I_{max} is the peak of phase current, defined as:

$$I_{\max} = \begin{cases} \frac{1}{1+K_\phi} K_i A \pi r_r \frac{D_0}{2m_1 N_t} & (RF-PMSM) \\ \frac{1}{1+K_\phi} K_i A \pi \frac{1+r_a}{2} \frac{D_0}{2m_1 N_t} & (AF-PMSM) \end{cases}, \tag{3}$$

where A is the total electric loading and K_Φ is the ratio of the electric loading on the rotor and stator.

K_p is the electrical power factor and it can be expressed as:

$$K_p = \frac{1}{T}\int_0^T \frac{e(t)\times i(t)}{E_{\max}\times I_{\max}} dt = \frac{1}{T}\int_0^T f_e(t) f_i(t) dt, \tag{4}$$

where $f_e(t)$ and $f_i(t)$ are defined as the normalized EMF and current waveforms.

K_i is the current waveform factor and is defined as:

$$K_i = \frac{I_{\max}}{I_{rms}} = \left[\frac{1}{T}\int_0^T \left(\frac{i(t)}{I_{\max}}\right)^2 dt\right]^{-1/2}. \tag{5}$$

To obtain the general-purpose sizing equation of the radial and axial flux machines, all previous equations from Eq. (1) to Eq. (5) must be combined; the result is expressed by Eq. (6):

$$P_{out} = \begin{cases} \frac{1}{1+K_\phi}\frac{m}{m_1}\frac{\pi}{2} K_e K_i K_p K_L \eta B_g A \frac{f}{p} r_r D_0^2 L_e \\ \frac{1}{1+K_\phi}\frac{m}{m_1}\frac{\pi}{2} K_e K_i K_p K_L \eta B_g A \frac{f}{p} (1-r_a^2)(\frac{1+r_a}{2}) D_0^2 L_e \end{cases}. \tag{6}$$

The studied topologies of the radial and axial flux machines have different shapes of slots. The designs of the two machines' slots models are presented in Figure 2.

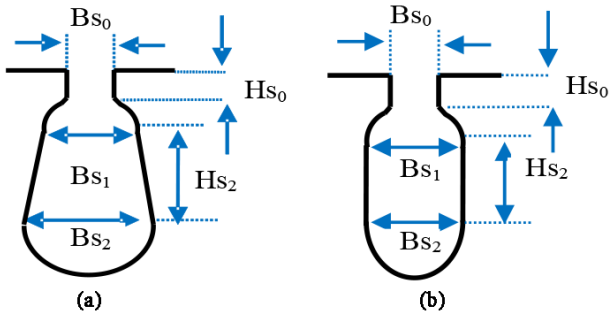

Figure 2. Slot dimensions: a) RF-PMSM, b) AF-PMSMS.

The dimensions of the respective slots models for the radial flux PMSM and axial flux PMSM are presented in Table 1.

The common parameters of the radial and axial flux machines such as the stator and rotor dimensions, the winding architecture, and the PM volume are presented. The two machines have common characteristics for

Table 1. RF-PMSM and AF-PMSM stator slot dimension values.

Slot dimensions	RF-PMSM	AF-PMSM
Hs_0 (mm)	0.5	1
Hs_2 (mm)	10.8	14.7
Bs_0 (mm)	2.5	2.5
Bs_1 (mm)	5.65	7.2
Bs_2 (mm)	8.5	7.2

Table 2. RF-PMSM and AF-PMSM design specifications.

	Parameters	PMSM-RF	PMSM-AF
Stator	L (mm)	65	30
	D_{in} (mm)	75	70
	D_{out} (mm)	120	
Rotor	L (mm)	65	15
	D_{in} (mm)	26	70
	D_{out} (mm)	74	120
Winding	Winding layer	1	2
	Conductors/slots	81	48
	Coil pitch	1	3
	Wire size (mm)	0.767	1.15
PM	Thickness (mm)	3.5	8

dimensioning the outer diameter of the stator and the rotor (120 mm), the steel type (M19_24G), the stacking factor (0.95), the magnet type (XG196/96), and the magnet embrace (0.7). In Table 2 the different design parameters are presented.

The surface-mounted radial flux machine and the single-sided axial flux machine can operate at a rated speed of 1500 rpm for a rated power of 550 W. Both machines dispose of 8 poles and 1 mm of air gap. The different electrical parameters are listed in Table 3.

The radial flux machine has a 24-slot stator while the axial flux machine has an 18-slot stator. The winding configuration used is called nonoverlap winding [18]. This type of winding uses a concentrated coil with a coil pitch equal to 1 for the axial flux and equal to 3 for the radial flux machine, as presented in Figure 3.

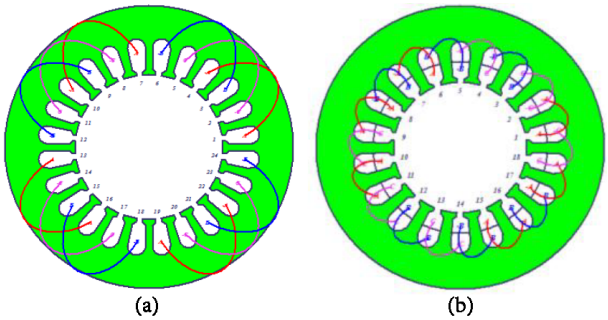

Figure 3. Stator winding configuration: a) RF-PMSM, b) AF-PMSM.

Table 3. RF-PMSM and AF-PMSM operating parameters.

Parameters	RF-PMSM	AF-PMSM
No. of poles (2p)	8	
No. of slots Z	24	18
No. of phases m	3	
Resistance	0.98 Ω	1.97 Ω
Phase connection	Y3	
Air gap	1 mm	
Rated power	550 W	
Rated speed	1500 rpm	
Rated voltage	127 V	
Frequency f	100 Hz	
Temperature	75 °C	

A double-layer nonoverlap winding [19] is used for the axial flux machine, which means that two coils are sharing one slot. With two coil layers per slot, all teeth are wound. For the studied RF-PMSM and AF-PMSM designs, there is a number of slots equal respectively to Z = 18 and Z = 24, and the number of poles is 2p = 8 and the number of phases is m = 3, so the number of slots per pole and per phase is:

$$q = \frac{Z}{2mp}, \tag{7}$$

which in this case is q = 1 for the RF-PMSM and q = 0.75 for the AF-PMSM.

The ratio between the number of phases and the number of slots is given by:

$$r = \frac{Z}{m}. \tag{8}$$

3. Finite element modeling

The single-sided AF-PMSM and the RF-PMSM are modeled in a 3D environment for two main reasons; the first is due to the disk-type shape of the axial flux topology, which is unlike the conventional radial flux machine, so by studying both in 3D we can investigate the magnetic behavior around the axial and radial axis. The second reason is the accuracy that 3D FE analysis offers compared to the 2D method or the analytical one. Nonetheless, using this method, no electromagnetic elements are neglected.

The studied machines are multipole rotating machines, and for time consumption reasons, the electromagnetic analysis can be reduced to an even number of poles by employing periodic boundary conditions. The RF-PMSM model presented in Figure 4a is divided into one quarter in order to accelerate the simulation time, but the obtained results and values will consider the full model of the machine. The AF-PMSM model in our study, shown in Figure 4b, is divided into half to accelerate the simulation time, but the result curves and values will also consider the complete model of the machine.

In order to apply the excitation and move to the postprocessing phase, the described model must be discretized by employing a meshing strategy. The mesh density must obey the accuracy versus time of simulation needs. The different parts of the machines are meshed separately with different resolutions. As an example, the

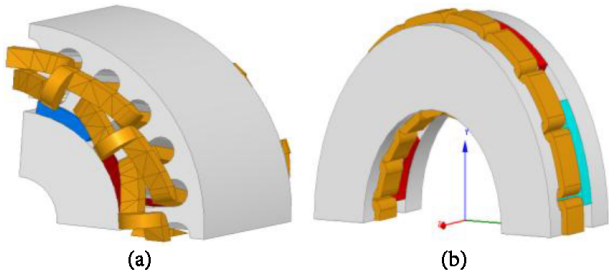

Figure 4. The studied 3D model of: a) RF-PMSM, b) AF-PMSM.

tetrahedral meshing for the radial flux machine in Figure 5a needs 15,490 tets for the active parts and 21,503 tets for the different regions, while the tetrahedral meshing for the axial flux PMSM presented by Figure 5b needs 11,011 tets for the active parts and 13,683 tets for the different regions. Due to its compact shape, the axial flux machine uses fewer meshing elements, thus consuming less simulation time.

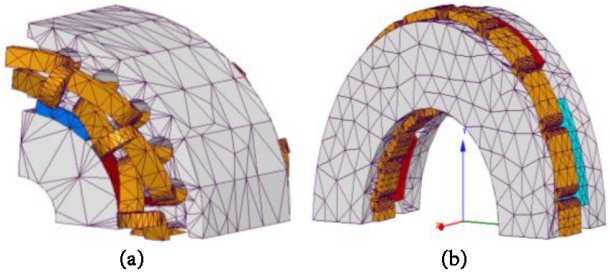

Figure 5. Meshing of the: a) RF-PMSM, b) AF-PMSM.

The different materials designated for the machines are assigned from the ANSYS library. The iron core for the stator and rotor are the same, named M19_24G, with a mass density of 7650 kg/m^3, and this electrical steel has a stacking factor of 0.95. The permanent magnets used are NdFeB type with code name XG196/96 with 1.10716 relative permeability and magnitude equal to –690,000 A/m. The coil material type is copper with bulk conductivity of 58 $\times$ 10^6 S/m.

4. Electromagnetic analysis

The postprocessing process consists of analyzing the magnetic field plots of the studied machines generated by the solver based on the finite element method. Figure 6a shows the magnetic flux density distribution for the radial flux machine model at the rated speed. It can be seen that there are no major saturation zones but higher distribution flux density values are essentially in the stator part. In Figure 6b the magnetic flux density distribution for the axial flux machine model at the rated speed shows that there are specific saturation zones inside the stator slots due to the concentration of the coils sharing those slots, but the overall flux density distribution values are lower than those of the radial flux machine.

The flux density in the air gap for one rotor cycle shows that the radial flux machine has better flux density in the cylindrical air gap than the axial flux machine. This can confirm the magnetic flux density distribution previously presented.

The eddy current losses are generated in the permanent magnets of the axial and radial flux machines. The computation of the magnetic field distribution is necessary for design purposes. The magnetic field strength

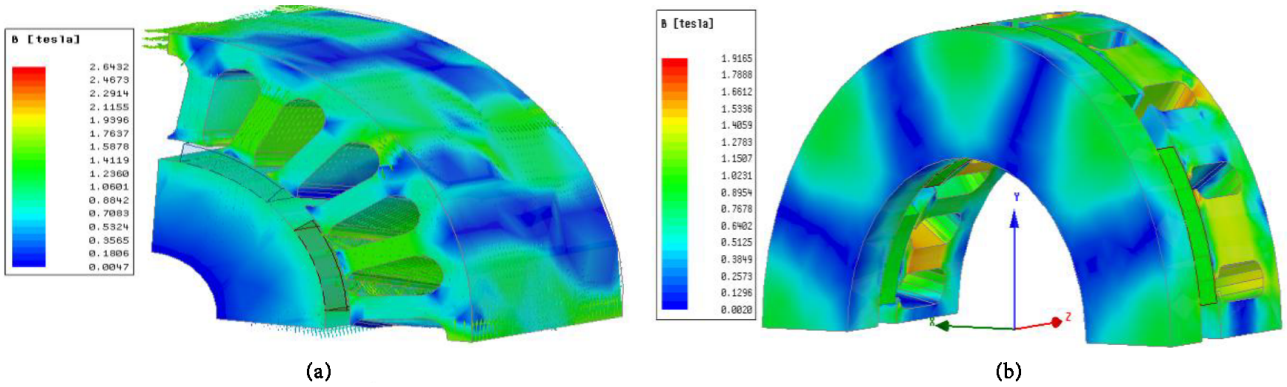

Figure 6. Magnetic flux density: a) RF-PMSM, b) AF-PMSM.

for the radial flux machine as presented in Figure 7a has a more saturated area than the axial flux machine in Figure 7b, especially around the magnets edges, which will generate eddy current losses in the stator conductors.

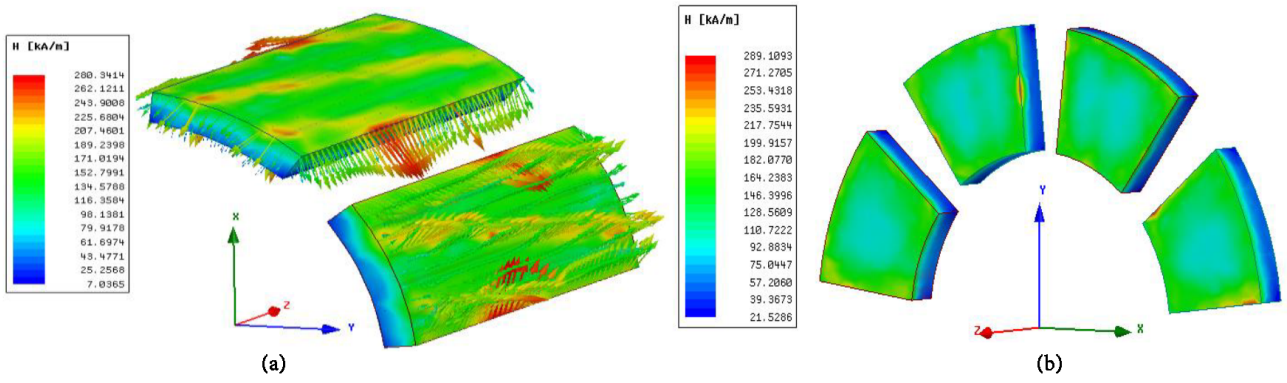

Figure 7. The magnetic field strength of: a) RF-PMSM, b) AF-PMSM.

The output torque of the radial and axial flux PMSMs is shown in Figure 8. The AF-PMSM has slightly better torque and less undulation than the RF-PMSM, but considering the volume difference between the two machines, this torque difference cannot be an advantage for the radial flux machine.

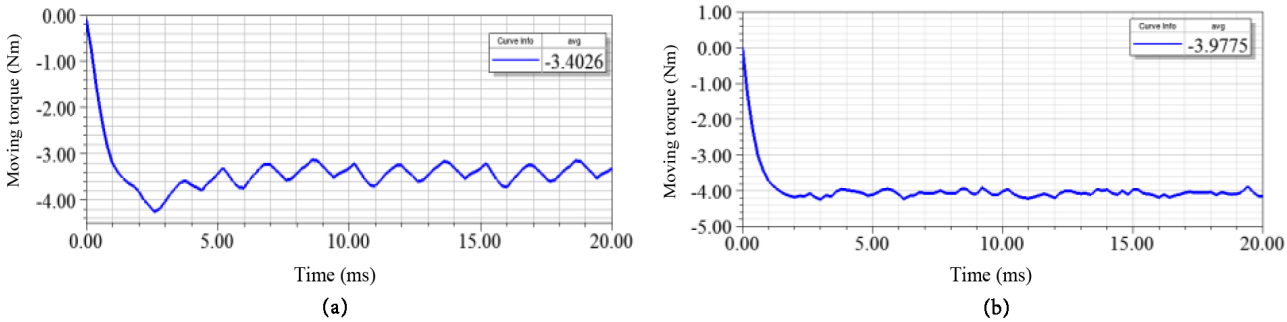

Figure 8. Evolution of the output torque for: a) RF-PMSM, b) AF-PMSM.

The evolution of the three-phase stator current and the induced voltages for the axial flux and radial flux machines are show in Figures 9 and 10.

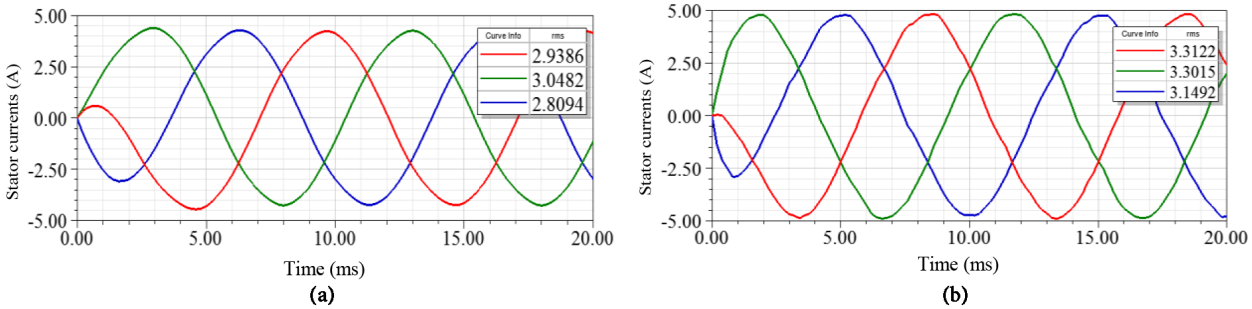

Figure 9. Evolution of the stator current for: a) RF-PMSM, b) AF-PMSM.

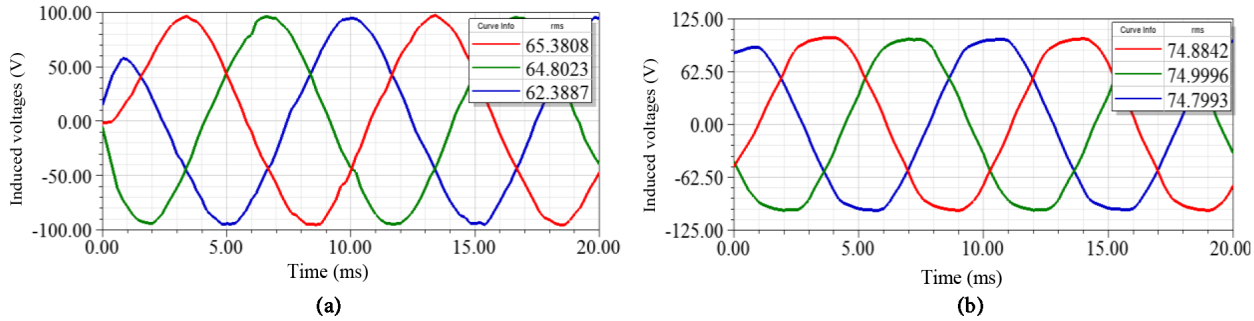

Figure 10. Evolution of the EMF for: a) RF-PMSM, b) AF-PMSM.

The core (iron) and solid (copper) losses of the radial flux and axial flux PMSMs are presented in Figure 11. The core losses representing the evolution of the loss in steel lamination used for the rotor and stator of the two machines clearly indicate that the radial flux machine has more core losses than the axial flux machine.

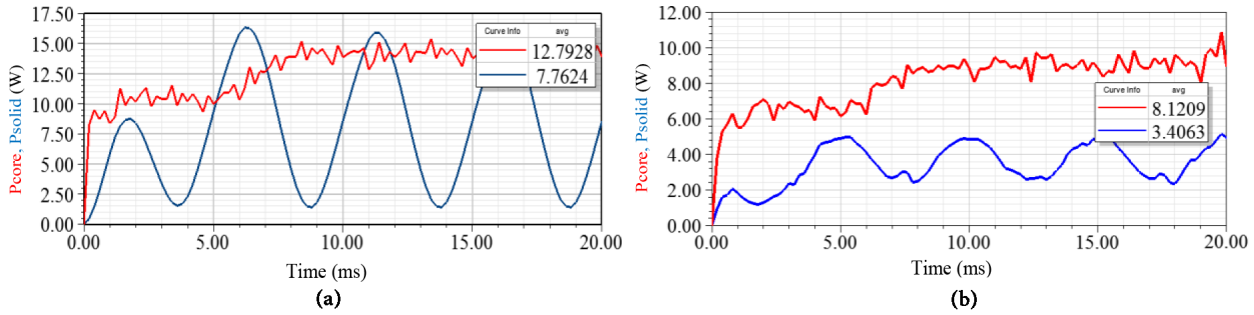

Figure 11. Evolution of the core and solid losses for: a) RF-PMSM, b) AF-PMSM.

In Figure 12, the eddy current and hysteresis losses are presented. Again in this case, the RF-PMSM has more power loss in magnetic active parts than the AF-PMSM.

For numerical computation of the cogging torque, the 3D FEM models of both machines are considered. The computation is conducted in the meshed area containing a closed path in the air gap around the stator in order to define the magnetic force F applied on the stator, which is based on the Maxwell stress tensor method [20].

Figure 13 presents the computed cogging torque of the axial flux and radial flux PMSMs. It can be observed that the axial flux machine has lesser cogging torque (0.396 Nm) than the radial flux machine (0.801 Nm). This result gives the axial flux machine the advantage for wind power applications.

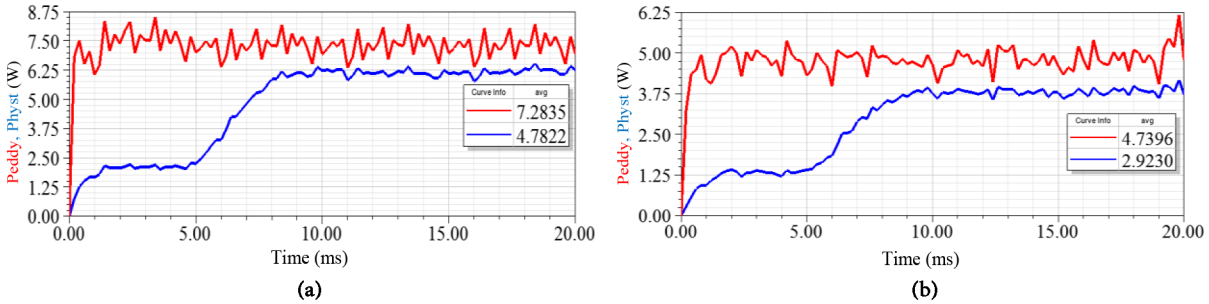

Figure 12. Evolution of the eddy current and hysteresis losses: a) RF-PMSM, b) AF-PMSM.

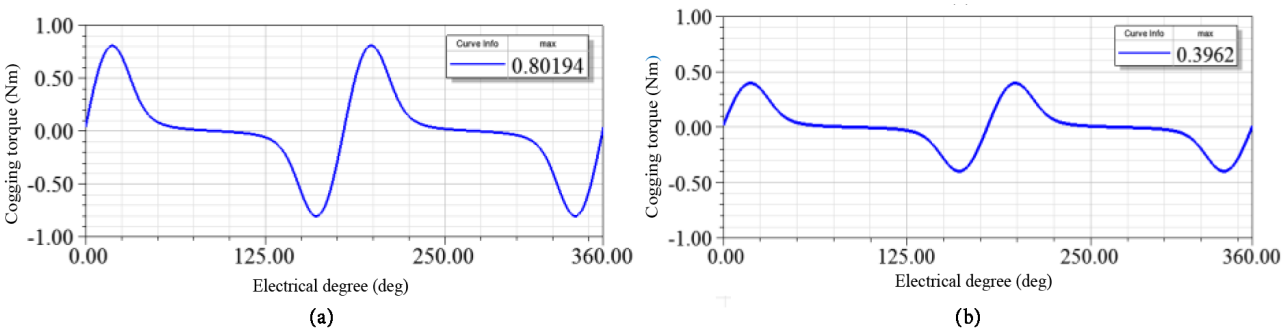

Figure 13. The cogging torque waveform: a) RF-PMSM, b) AF-PMSM.

5. Performance evaluation and discussion

The overall system performance of the surface-mounted radial flux and slotted single-sided axial flux PMSM is compared in Table 4. Both machines have the same pole number (p = 8) and operate at the same speed (1500 rpm) and at 100 Hz. It can be seen that the axial flux configuration has a better torque-to-weight ratio and has less loss in the iron core, as in the winding configuration, than the radial flux topology.

Table 4. Performance comparison between radial and axial flux machines.

	RF-PMSM	AF-PMSM
RMS current (A)	3	7.8
Avg. torque (Nm)	3.4	3.9
Loss in iron core (W)	12.7	8.1
Solid loss (W)	7.7	3.4
Eddy current loss (W)	7.2	4.7
Hysteresis loss (W)	4.7	2.9
Maximum saturation of the magnetic flux density B [T]	2.7	2.2
Maximum saturation of the magnetic field H [kA/m]	318.8	322.7
Cogging torque (Nm)	0.8019	0.3962
Efficiency %	88.8	90.4

As for the magnetic performances, the machines have different saturation zones, but the axial flux machine has less saturation density in the stator and rotor core than the radial flux. The magnetic field saturations for

the permanent magnets on the cylindrical rotor of the radial flux are spread around the edges, which can lead to demagnetization incidents. Both losses and saturations have a direct impact on the radial and axial flux machines' efficiencies. In this case, however, the axial flux machine has better efficiency compared to the radial flux machine. The material consumption of the active parts for both machines is listed in Table 5. The slotted single-sided axial flux machine uses less steel and copper than the radial flux, but it consumes more permanent magnets. On the other hand, the radial flux machine is heavier than the axial flux due to its cylindrical shape, which needs more material in the conception process. From a construction point of view, the axial flux machine is easier to manufacture than the radial one. In fact, the manufacturing cost is half the cost of the active materials, which explains the factor (k = 1.5). For estimating the cost of both machines, the market indicates that the copper is rated at 8 €/kg, the PM is rated at 50 €/kg, and the iron is rated at 3 €/kg [21].

Table 5. Material consumption comparison between radial and axial flux machines.

	RF-PMSM	AF-PMSM
Armature copper density (kg/m^3)	8900	
Permanent magnet density (kg/m^3)	7800	
Armature core steel density (kg/m^3)	7650	
Rotor core steel density (kg/m^3)	7650	
Copper weight (kg)	1.31	0.54
Permanent magnet weight (kg)	0.31	0.32
Stator core weight (kg)	5.3	1.62
Rotor core weight (kg)	1.7	0.81
Total weight (kg)	7	2.43
Manufacturing coefficient k	2	1.5
Estimated cost (€)	94	41

6. Conclusion

In this paper, two 550-W axial flux and radial flux wind turbine topologies were considered in order to analyze and compare their performances. The modeling was divided into three phases. In the first, the dimensioning of the output power of both machines was presented using the sizing equation. Then the design specification of the radial and axial machines was presented, including the parameters in common such as the outer diameter and the different parameters for the stator, rotor, windings, and permanent magnet. The third phase consisted of studying the 3D model of the proposed machines using the finite element approach. The postprocessing results led us to conclude the following: the flux density distribution in the axial flux machine encountered less saturation than the radial flux machine. In addition, the magnetic field strength in the PMs of the radial flux machine endured more saturation, which generated more eddy current losses in the stator winding armature. Furthermore, the torque for the axial flux machine has better value and less undulation than the radial flux machine. As for the material consumption, the axial flux machine volume is nearly half that of the radial flux machine, which offers a higher torque-to-weight ratio, and, as a consequence, the axial flux machine can be cheaper than the radial flux machine.

References

[1] Qu R, Liu Y, Wang J. Review of superconducting generator topologies for direct-drive wind turbines. IEEE T Appl Supercon 2013; 23: 5201108-5201108.

[2] Jumayev S, Paulides JJH, Boynov KO, Pyrhonen J, Lomonova EA. 3-D analytical model of helical winding PM machines including rotor eddy-currents. IEEE T Magn 2016; 99: 1-8.

[3] Chen A, Nilssen R, Nysveen A. Performance comparisons among radial-flux, multistage axial-flux, and three-phase transverse-flux PM machines for downhole applications. IEEE T Ind Appl 2010; 46: 779-789.

[4] Chen Y, Fu WN, S HL, Liu H. A quantitative comparison analysis of radial-flux, transverse-flux, and axial-flux magnetic gears. IEEE T Magn 2014; 50: 1-4.

[5] Zhao W, Lip AT, Kwon B. Comparative study on novel dual stator radial flux and axial flux permanent magnet motors with ferrite magents for traction application. IEEE T Magn 2014; 50: 1-4.

[6] Ishikawa T, Amada S, Segawa K, Kurita N. Proposal of a radial- and axial-flux permanent magnet synchronous generator. IEEE T Magn 2017; 53: 1-4.

[7] Sorgdrager AJ, Grobler AJ. Influence of magnet size and rotor topology on the air-gap flux density of a radial flux PMSM. In: IEEE 2013 International Conference on Industrial Technology Conference; 25–28 February 2013; Cape Town, South Africa. New York, NY, USA: IEEE. pp. 337-343.

[8] Guo B, Huang Y. A fast analytic model of axial flux permanent magnet machines with static/dynamic axis eccentricity. J Magn 2016; 21: 554-560.

[9] Foglia G, Di Gerlando A, Perini R, Iacchetti M. Parasitic currents in stray paths of some topologies of YASA AFPM machines: trend with machine size. IEEE T Ind Electron 2016; 99: 2746-2756.

[10] Yeşilbağ E, Ertuğrul Y, Ergene L. Axial flux PM BLDC motor design methodology and comparison with radial flux PM BLDC motor. Turk J Elec Eng & Comp Sci 2017; 27: 3455-3467.

[11] Chan TF, Wang W, Lai L. Performance on an axial-flux permanent magnet synchronous generator from 3-D finite element analysis. IEEE T Energy Conver 2010; 25: 269-276.

[12] Parviainen A, Niemela M, Pyrhonen J, Mantere J. Performance comparison between low-speed axial-flux and radial-flux permanent magnet machines including mechanical constraints. In: IEEE 2005 International Conference on Electric Machines and Drives; 15–18 May 2005; San Antonio, TX, USA. New York, NY, USA: IEEE. pp. 1695-1702.

[13] Huang S, Jian L, Lionardi F, Lipo LA. A comparison of power density for axial flux machines based on general purpose equations. IEEE T Energy Conver 1999; 14: 185-192.

[14] Steentjes S, Boehmer S, Hameyer K. Permanent magnet eddy-current losses in 2-D FEM simulations of electrical machines. IEEE T Magn 2015; 51: 1-4.

[15] Bohmer S, Lange E, Hafner M, Cramer T, Bischof C, Hameyer K. Mesh decomposition for efficient parallel computing of electrical machines by means of FEM accounting for motion. IEEE T Magn 2012; 48: 891-894.

[16] Bacchus A, Tounzi A, Argaud JP, Bouriquet B, Biet M, Macaire L, Le Menach Y. Estimation of FEM model parameters using data assimilation and Its application to an electrical machine. IEEE T Magn 2015; 99: 8101204.

[17] Guleç M, Yolaçan E, Demir Y, Ocak O, Aydın M. Modeling based on 3D finite element analysis and experimental study of a 24-slot 8-pole axial-flux permanent-magnet synchronous motor for no cogging torque and sinusoidal back-EMF. Turk J Elec Eng & Comp Sci 2016; 24: 262-275.

[18] Zhao W, Lip AT, Kwon B. Dual-stator two-phase permanent magnet machines with phase-group concentrated-coil windings for torque enhancement. IEEE T Magn 2015; 51: 1-4.

[19] Jung J, Hofmann W. Comparison of two concentrated winding topologies applied on an axial flux permanent magnet machine. In: 2015 17th European Conference on Power Electronics and Applications; 8–10 September 2015; Geneva, Switzerland. pp. 1-10.

[20] Hemaida A, Hannon B, Vansompel H, Sergeant P. Comparison of three analytical methods for the precise calculation of cogging torque and torque ripple in axial flux PM machines. Math Probl Eng 2016; 2016: 1-14.

[21] Du-Bar T, Landmark S, Alatalo M. An electric machine design procedure that includes multiple cost scenarios. In: 2016 18th European Conference on Power Electronics and Applications; 5–9 September 2016; Karlsruhe, Germany. pp. 1-9.